Hindawi Publishing Corporation
Journal of Spectroscopy
Volume 2015, Article ID 493607, 10 pages
http://dx.doi.org/10.1155/2015/493607

Research Article

Excitation Induced Tunable Emission in Ce^{3+}/Eu^{3+} Codoped $BiPO_4$ Nanophosphors

Sarabjot Singh,[1,2] G. Lakshminarayana,[2,3] Manoj Sharma,[1] Thang Duy Dao,[2,3] K. Chen,[2,3] Yoshiki Wada,[4] T. Takeda,[5] and T. Nagao[2,3]

[1]*Department of Nanotechnology, Sri Guru Granth Sahib World University, Fatehgarh Sahib, Punjab 140406, India*
[2]*International Center for Materials Nanoarchitectonics (MANA), National Institute for Materials Science (NIMS), 1-1 Namiki, Tsukuba, Ibaraki 305-0044, Japan*
[3]*CREST, Japan Science and Technology Agency, 4-1-8 Honcho, Kawaguchi, Saitama 332-0012, Japan*
[4]*Environment and Energy Materials Division, National Institute for Materials Science, 1-1 Namiki, Tsukuba, Ibaraki 305-0044, Japan*
[5]*Nitride Particle Group, Nano Ceramics Center, National Institute for Materials Science (NIMS), Namiki 1-1, Tsukuba, Ibaraki 305-0044, Japan*

Correspondence should be addressed to Manoj Sharma; manojnarad@gmail.com and T. Nagao; nagao.tadaaki@nims.go.jp

Received 23 November 2014; Revised 16 February 2015; Accepted 23 February 2015

Academic Editor: Damien Boyer

Ce^{3+}, Eu^{3+} ions singly doped, and Ce^{3+}/Eu^{3+} codoped bismuth phosphate ($BiPO_4$) nanophosphors were synthesized by a simple precipitation method and their structural, morphological, and photoluminescence properties were investigated. The structural and morphological analysis confirms the pure hexagonal crystal structure of the synthesized nanophosphors. From the Fourier transform infrared (FTIR) spectra various absorption bands respective to functional groups such as PO4 and phonon vibrations including the bending modes of the PO_4 units are identified. The Ce^{3+} doped nanophosphors show spectrally broad luminescence in the blue (centred at 459 nm) wavelength region under the direct optical excitation of Ce^{3+} at 417 nm. For Eu^{3+} doped nanophosphors, five emission bands have been observed with 394 nm excitation wavelength. Among them, 595 nm has shown bright yellowish-orange emission. These results demonstrate that by appropriately tuning the excitation wavelength of these codoped nanophosphors the emission color in the visible region (blue and orange) can be flexibly controlled in a single sample without varying its chemical composition and size. The mechanism for this excitation energy dependent tunable emission is explained on the basis of nonenergy transfer (ET) occurring among Ce^{3+}/Eu^{3+} dopant ions.

1. Introduction

Recently, bismuth phosphate ($BiPO_4$) has received a great deal of research interest due to its potential applications in ion sensing [1], separating radioactive elements [2], catalysis [3, 4], and light emitting devices [5]. $BiPO_4$ is also useful for the improvement of electrical properties of the phosphate glasses, which are of technological interest as ionic, electronic, and fast ionic conductors [5, 6]. Recently for alleviating negative environment impact of toxic dyes and pollutants, $BiPO_4$ has shown better photocatalytic property in comparison to commercial Degussa P25 TiO_2 creating worldwide interest in the study of this material [6]. Various methods such as chemical vapor deposition [7], sonochemical method [8], and hydrothermal method [9] are reported to synthesize $BiPO_4$ but these methods show some drawbacks such as requiring relatively high temperatures, sharp thermal gradient, longer reaction times, and difficulty in controlling the final product structure. It is well known that bismuth phosphate ($BiPO_4$) exhibits three different crystal structures such as hexagonal phase (HP), low temperature monoclinic phase (LTMP), and high-temperature monoclinic phase (HTMP), respectively [10]. The hexagonal phase of hydrated $BiPO_4 \cdot xH_2O$ can be synthesized at room temperature through a wet chemical method [11].

Recently, due to comparable ionic radius of Bi^{3+} (1.11 Å) with that of lanthanide ions, $BiPO_4$ has drawn considerable interest as a host matrix for doping lanthanide ions for their

luminescent applications [12–14]. Both cerium and europium can be found in two oxidation states (Ce^{3+} and Ce^{4+}, and Eu^{2+} and Eu^{3+}) depending upon the preparation conditions [15]. Ce^{3+} absorption bands in the UV region originate from the transitions between the $^2F_{5/2}$ ground state and 5d energy levels. In 4+ oxidation state, cerium has no electron in the 4f level, so it shows no 4f–5d transition. The Ce^{4+} absorption is caused by the electron/charge transfer between the shell of the cerium ions and neighboring ions [16]. As a result, Ce^{4+} ions do not show any emission and excitation bands. Electron transitions between the energy levels of the Ce^{3+} ion can be studied by using photoluminescence excitation (PLE) and photoluminescence (PL) measurements. The spectrally broad Ce^{3+}: 5d $\rightarrow$ 4f luminescence band produces emission colors ranging from deep blue to red, depending on the type and composition of the host matrix [17–20]. Among the lanthanide ions, trivalent europium (Eu^{3+}) is well known to give rise to the intense orange-red luminescence. Generally, the luminescent properties of phosphors are strongly dependent on the crystal structure of the host materials. Europium ions are known to be good spectroscopic probes in different host materials due to its $^{2S+1}L_J$ multiplets structure with nondegenerate first excited and ground levels, $^5D_0$ and $^7F_0$, respectively. Also, the number of Stark components and intensity ratio of the $^5D_0 \rightarrow {}^7F_J$ transitions are useful in understanding the symmetry at the Eu^{3+} site [21]. The Eu^{3+} ion has the lowest excited level ($^5D_0$) of the $4f^6$ configuration which is situated below the $4f^5$5d configuration that shows very sharp lines extending from visible to the near-infrared depending on the host matrix.

Due to the wide range of applications, the development of nanostructured lanthanide ions doped $BiPO_4$ and the investigation of their functional properties could be an important research topic. Generally in rare earth codoped nanophosphors energy transfer among rare earth ions is studied with the aim to enhance emission of activator ion by efficient energy transfer from other dopant ions acting as sensitizer. Recently different groups have shown excitation wavelength dependent tunable emission in various organic-inorganic hybrid quantum dots [22, 23], mixed lanthanide complexes [24], nanocolloids of ZnO [25], CdSe/ZnS quantum dots [26], graphene oxide [27], and lanthanide doped metal organic frameworks [28]. All these reports have shown that these different systems show tunable emission in visible color just by varying the excitation wavelength without changing its chemical composition or size. They have used these materials for multicolor bioimaging applications, white light emission, and different color display applications. In the present work, the Ce^{3+} and Eu^{3+} singly doped and Ce^{3+}/Eu^{3+} codoped $BiPO_4$ nanophosphors were synthesized by a facile precipitation method using oleic acid as a capping agent. Here we highlight the excitation wavelength dependent tunable emission behavior of codoped $BiPO_4$ nanophosphors. Possible mechanism for this tunable emission in single sample is explained by nonenergy transfer process in Ce^{3+} and Eu^{3+} dopants ions in host $BiPO_4$.

2. Experimental

2.1. Synthesis of Lanthanide Ions Doped $BiPO_4$. For the preparation of Ce^{3+}, Eu^{3+} singly doped and Ce^{3+}/Eu^{3+} codoped $BiPO_4$ nanophosphors, $Bi(NO_3)_3{\cdot}5H_2O$ (99.9%), $Eu(CH_3CO_2)_3{\cdot}4H_2O$ (99.9%), and $CeN_3O_9{\cdot}6H_2O$ (99.9%) were used as starting materials. All chemicals were of reagent grade and used as received without further purification. Firstly, prerequisite amount of $Bi(NO_3)_3{\cdot}5H_2O$ was dissolved in concentrated HCl in a beaker and excess of acid was evaporated out repeatedly by adding water. To this solution the required amount of lanthanide salts was added along with 20 mL oleic acid and it was transferred into a two-necked round bottom flask. The synthesis of well dispersed $BiPO_4$ nanocrystals in oleic acid (OA) and bis(2-ethylhexyl) phosphate (BEHP) media by a high-temperature hydrolysis reaction has also been reported by other researchers [29]. Here in our synthesis, we used oleic acid as both solvent and surfactant. An aqueous solution (3 mL) of ammonium dihydrogen phosphate (ADP, 0.3 g) was added while stirring as a phosphate source. The solution was maintained for two hours at 100°C while continuously stirring. The solid precipitate and liquid contents were separated by centrifugation. Finally, the precipitate obtained was washed with methanol and acetone repeatedly several times to remove unreacted species and dried under ambient conditions. The synthesized five samples in this work in their nominal compositions are 99.0 mol% $BiPO_4$: 1.0 mol% Eu^{3+}, 95.0 mol% $BiPO_4$: 5.0 mol% Ce^{3+}, 97.0 mol% $BiPO_4$: 0.5 Eu^{3+}/2.5 Ce^{3+} (mol%), 94.0 mol% $BiPO_4$: 1.0 Eu^{3+}/5.0 Ce^{3+} (mol%), and 94.0 mol% $BiPO_4$: 5.0 Eu^{3+}/1.0 Ce^{3+} (mol%), respectively.

2.2. Characterization. The powder X-ray diffraction (XRD) profiles were obtained on a Rigaku X-ray diffractometer (model Rint 2000) with Cu-K_α (λ = 1.542 Å) radiation using an applied voltage of 40 kV and 40 mA anode current, calibrated with Si at a rate of 2 deg/min. The surface morphology of the prepared bismuth phosphate samples was observed by scanning electron microscopy (SEM; S-4800 HITACHI Company) at 1 nm resolution and an acceleration voltage of 5 kV, together with the X-ray energy dispersive spectroscopy (EDS; equipped on SU8000 HITACHI SEM) for chemical analysis. Transmission electron microscopy (TEM/HRTEM) measurements (bright field low magnification and lattice imaging) were performed using 200 keV (model JEM-2100F JEOL company) TEM microscope. The Fourier transform infrared (FTIR) spectra of the phosphors were measured in the transmission mode over the 100–1400 cm^{-1} range by a Thermo Nicolet NEXUS-670 FTIR machine using solid substrate beam splitter and DTGS polyethylene detector with a spectral resolution of ~4 cm^{-1}. The room temperature photoluminescence excitation (PLE) spectra and photoluminescence (PL) spectra were measured by using JASCO Fluorescence Spectrometer FP8500 system, having a 150 W Xe lamp as the excitation source. Around 10 mg sample powder was mixed with two drops of methanol, made into a slurry and spread over a glass plate, and dried under ambient conditions prior to luminescence measurements.

The excitation and detection geometry was fixed, and samples were mounted reproducibly to allow for quantitative comparison of the relative fluorescence intensity between different phosphor samples. All emission spectra were corrected for the detector response and all excitation spectra for the lamp profile. All the PLE and PL measurements were carried out with a resolution of 5 nm.

3. Results and Discussion

The phase and purity of the samples were examined by X-ray power diffraction (XRD) measurement and Figure 1(a) presents the XRD profiles 1.0 mol% Eu^{3+}, 5.0 mol% Ce^{3+}, and 1.0 Eu^{3+}/5.0 Ce^{3+} (mol%) doped $BiPO_4$ nanophosphors. For comparison purpose we have also given the XRD profile of pure hexagonal phase $BiPO_4$ (JCPDS 45-1370) [4]. From these profiles one can see that all of the samples prepared were in good agreement with the standard data of the pure hexagonal phase $BiPO_4$ [4]. No impurity peaks were observed in these XRD patterns, indicating high purity of the synthesized samples. The intense and sharp diffraction peaks suggested that the as-synthesized products were well crystallized. It is well known that in hexagonal phase of $BiPO_4$, Bi^{3+} ions are surrounded by eight nearest neighbor oxygen atoms forming square antiprism geometry around Bi^{3+} [30]. To check whether the lanthanide ions (Eu^{3+} or Ce^{3+}) are successfully incorporated into the host lattice by substituting the Bi^{3+} ions or if they occupy the interstitial or surface sites of the $BiPO_4$ host, we have selected the high intensity peak (2 0 0) of pure $BiPO_4$ hexagonal phase from Figure 1(a) and compared it with doped nanophosphors. A careful comparison of the (2 0 0) diffraction peaks in the range of $2\theta = 29.1^\circ$–29.9° (Figure 1(b)) showed that the peak position of Eu^{3+} doped sample is shifted slightly towards a higher 2θ value. This can be attributed to the smaller ionic radius of Eu^{3+} (1.066 Å) as compared to Bi^{3+} (1.11 Å) and therefore associated with lattice contraction. But in the case of Ce^{3+} doped sample, the (2 0 0) peak is slightly shifted to a lower 2θ value and this can be ascribed to the higher ionic radius of Ce^{3+} (1.143 Å) compared to Bi^{3+} (1.11 Å) and thus related to the lattice expansion. For the Ce^{3+}/Eu^{3+} codoped sample, one can see the effect of Eu^{3+} on the Ce^{3+} ion as the (2 0 0) peak very slightly shifts to higher 2θ with apparent sharpness. This confirms the incorporation of either Ce^{3+} or Eu^{3+} ions into the lattice of $BiPO_4$. The morphology of the Eu^{3+} doped $BiPO_4$ nanophosphor was analyzed by scanning electron microscopic technique and Figure 2(a) depicts the typical SEM image of the Eu^{3+} doped $BiPO_4$ sample which shows that the product is composed of well-dispersed hexagonal structures. The length of these smooth surfaced hexagonal structures ranges from 200 to 400 nm and most of them are above 200 nm with diameter approximately ranging from 50 to 200 nm. The measured EDAX profiles of all the synthesized samples are presented in Figures 2(b) to 2(f). The measurements confirm the presence of the main constituents Bi, P, O, Eu, and Ce in the respective lanthanide doped nanophosphors. No compositional variation was found upon probing different locations within each sample, indicating that the observed elements are homogeneously distributed in the crystalline matrices. Table 1 summarizes the elemental compositional data derived from Figures 2(b) to 2(f). The morphology and size of the Eu^{3+} doped sample were further examined by transmission electron microscopy (Figure 3(a)). It shows the production of uniform $BiPO_4$ hexagonal nanostructure with diameter around 200 nm. Further the TEM measurements show that the doping with different lanthanide ions actually did not change the morphology of the nanostructures if they were synthesized in a similar way. Elemental mapping of Bi, P, O, and Eu of the nanostructure (Figure 3(a)) was carried out by energy dispersive X-ray spectroscopy and from Figure 3(e) it is clearly seen that Eu is doped into $BiPO_4$ with uniform and smooth morphology. The electron diffraction (ED) pattern (scale bar is 5 nm) of a selected nanostructure (Figure 3(f)) revealed a regular and bright spots array, indicating that the nanostructures are crystals with a preferential growth orientation along the (110) crystalline plane. These results show that the samples are high-quality crystals.

Table 1: Elemental composition data obtained from EDAX profiles of $BiPO_4$ doped with (a) 1.0 mol% Eu^{3+}, (b) 5.0 mol% Ce^{3+}, (c) 1.0 Eu^{3+}/5.0 Ce^{3+} (mol%), (d) 0.5 Eu^{3+}/2.5 Ce^{3+} (mol%), and (e) 5.0 Eu^{3+}/1.0 Ce^{3+} (mol%).

S.N.	Elements	Weight %	Atomic %
(a)	O(K)	37.27	81.77
	P(K)	7.94	8.99
	Eu(L)	0.58	0.13
	Bi(M)	54.21	9.11
(b)	O(K)	37.49	81.04
	P(K)	8.67	9.68
	Ce(L)	4.48	1.11
	Bi(M)	49.36	8.17
(c)	O(K)	28.16	73.80
	P(K)	8.78	12.32
	Ce(L)	3.38	1.05
	Eu(L)	1.58	0.74
	Bi(M)	58.10	12.09
(d)	O(K)	41.81	84.48
	P(K)	7.01	7.32
	Ce(L)	3.43	0.79
	Eu(L)	0.36	0.08
	Bi(M)	47.39	7.33
(e)	O(K)	34.28	79.39
	P(K)	8.27	9.89
	Ce(L)	1.74	0.46
	Eu(L)	5.76	1.41
	Bi(M)	49.95	8.86

FTIR spectroscopy allows identification of the different functional groups of the synthesized material's molecular structure and has been employed extensively for this purpose [31, 32]. Figure 4 shows well-resolved FTIR spectra of all the prepared nanophosphors in the 100–1400 cm^{-1} range. All the spectra show similar features regarding the respective

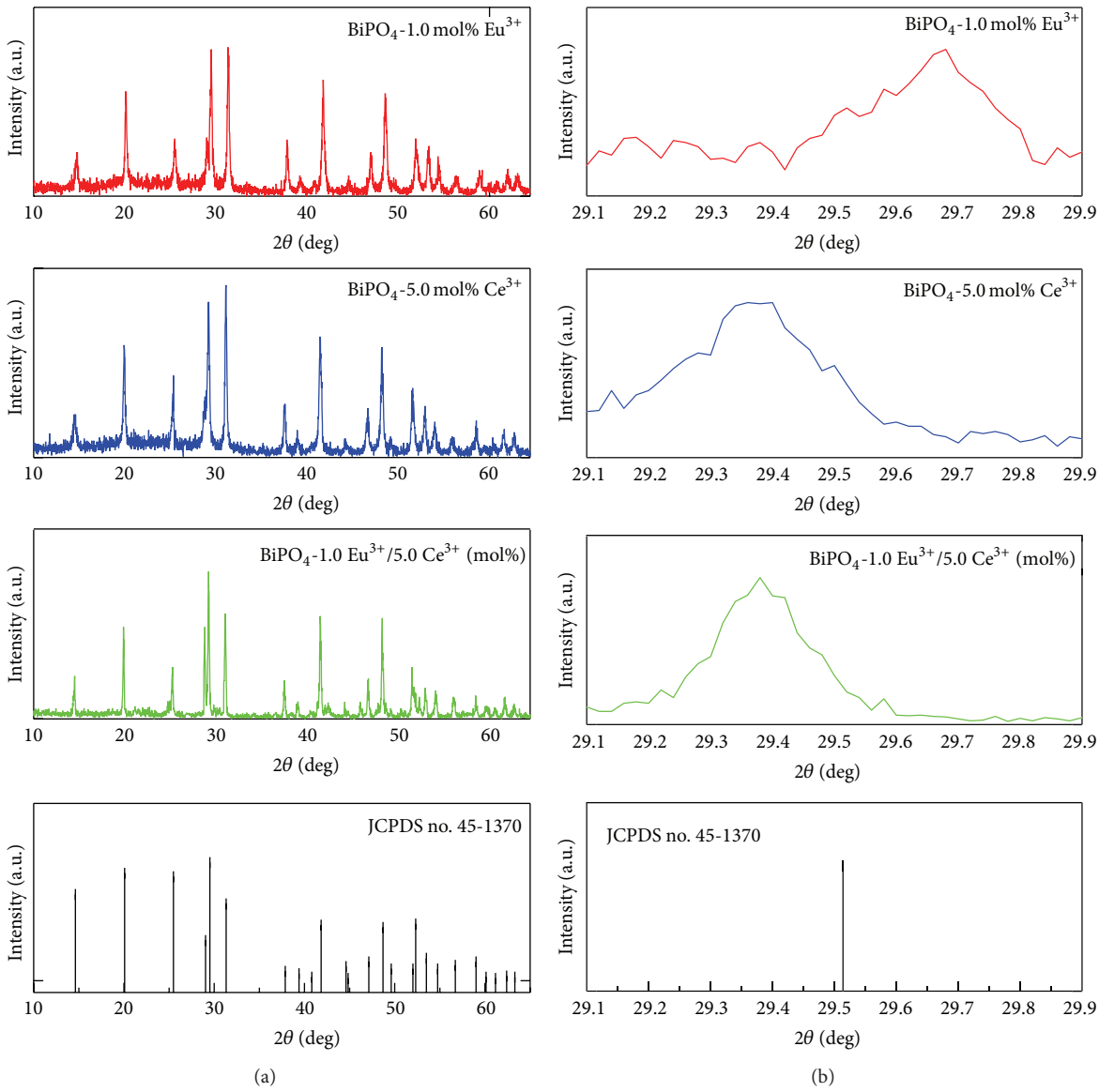

Figure 1: (a) XRD profiles of some of the synthesized samples, (b) XRD profiles in the range 29.1 to 29.9 (2 theta).

absorption bands. For 5.0 mol% Ce^{3+} doped sample the very intense band centered at 1057 cm^{-1} is due to the ν_3 stretching vibration of the PO_4 group. Several small intensity bands can also be seen in this region for other samples as the PO_4 group is situated in C_2 symmetry. For the hexagonal $BiPO_4$, the PO_4^{3-} groups are under C_2 symmetry [33, 34] and corresponding ν_1 and ν_3 modes of vibration are very close that they might overlap with each other significantly to give a peak around 1057 cm^{-1} (see Figure 4). The identified sharp bands at 596 and 536 cm^{-1} could be assigned to the vibrations δ(O–P–O) and ν_4 (PO_4), respectively [35, 36]. Two bands are observed at 475 and 377 cm^{-1} and are considered to have originated from the ν_2 bending modes of the PO_4 units. The band observed at 170 cm^{-1} for all the samples could be assigned to an OBiO symmetric bending mode [8]. Generally the phosphate group related modes could show either blue or red shift based on the crystal symmetry of the host and electronic charge balancing ion [13]. No band at 1250 cm^{-1} (ν(C–O)) is observed that can be related to oleic acid and H_2O adhered on the particle surface indicating during the drying process all the H_2O and OA are removed from the samples.

It is well known that Ce^{3+} with a $4f^1$ electron configuration has a $^2F_{J\,(J=5/2,7/2)}$ ground state and the 4f electrons can be photoexcited to 5d levels. The 5d levels are further split into various energy levels, depending on the crystal field strength of the host material [37]. The energy levels splitting patterns are determined by the chemical environment and the symmetry of the host matrix around the Ce^{3+} ions. Figure 5(a) presents the photoluminescence excitation (PLE) and photoluminescence (PL) spectra of the 5.0 mol% Ce^{3+} doped $BiPO_4$ nanophosphor. Direct excitation of Ce^{3+} occurs via the parity allowed $4f(^2F_{5/2}) \rightarrow$ 5d absorptions, which

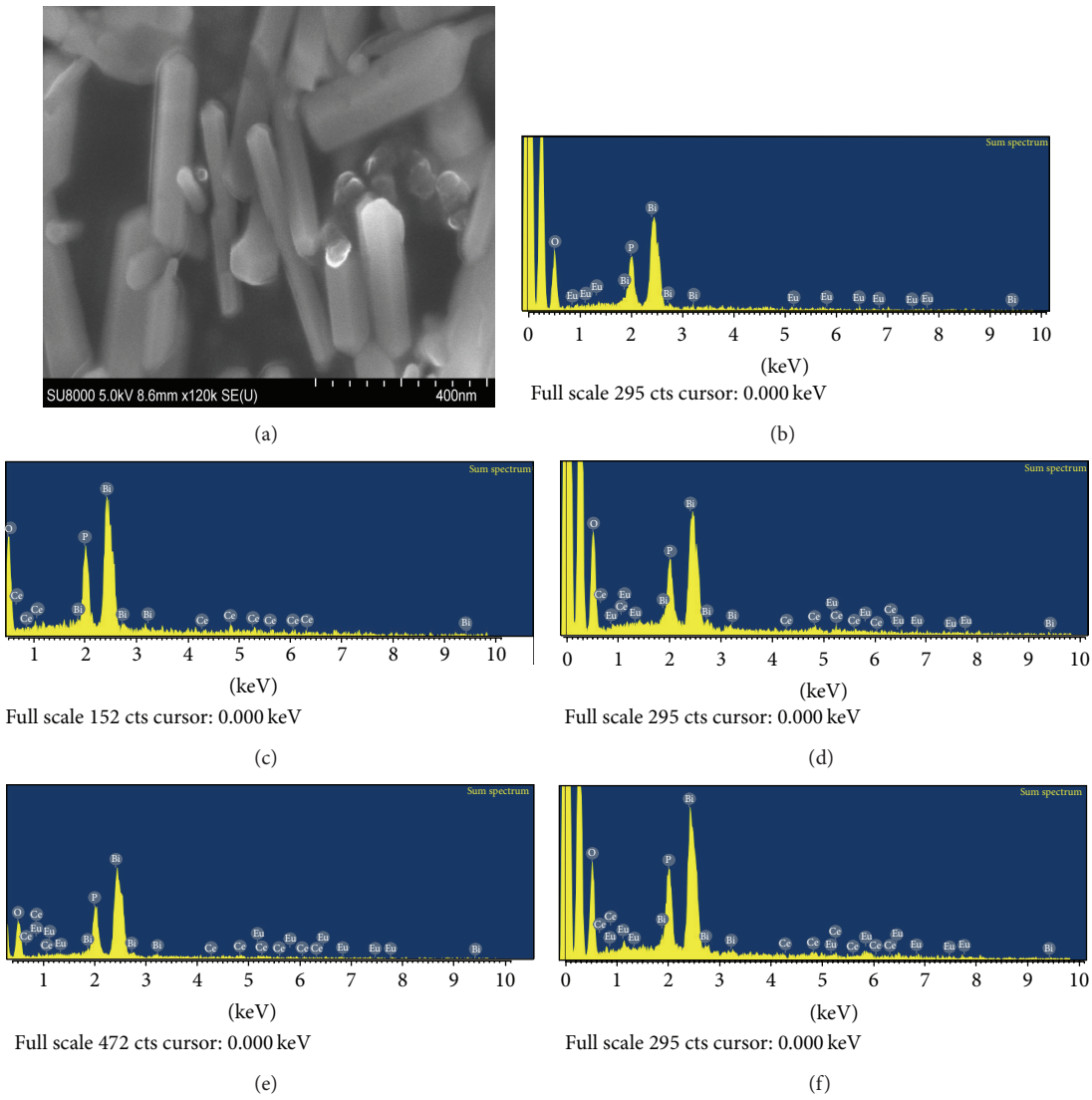

FIGURE 2: (a) SEM image of the 1.0 mol% Eu^{3+} doped sample, (b–f) EDAX profiles of all the synthesized samples.

are observed as a broad band centered at 417 nm in the PLE spectrum (Figure 5(a)). The excited Ce^{3+} ion then nonradiatively relaxes to the lowest-energy crystal-field level of the 5d state from where it decays radiatively to the $^2F_{7/2}$ and $^2F_{5/2}$ 4f multiplets of Ce^{3+} [38]. The respective PL spectrum of Ce^{3+} doped nanophosphor has shown a relatively sharp and asymmetric blue emission band extending from 450 to 470 nm and peaking at around 459 nm and which could be assigned to the 5d $\rightarrow$ $^2F_{7/2}$ transition. The energy difference ~2194 cm^{-1} between 417 nm and 459 nm can be well matched with the energy difference between the two spin orbit split components $^2F_{5/2}$ and $^2F_{7/2}$ of Ce^{3+}. Generally, in noncrystalline materials one can observe broad emission band for cerium ion (Ce^{3+}) extending from blue to green wavelength region or even covering entire visible wavelength region in some other noncrystalline or crystalline host materials. In [14], very broad emission from hexagonal $BiPO_4$ doped with cerium ion has been reported. In our case, the sharpness of the cerium emission band could be due to the incorporation of Ce^{3+} ion into Bi^{3+} crystal site in $BiPO_4$ as confirmed by the XRD. In Figure 5(b) the relevant Ce^{3+} ion energy level diagram is presented and the excitation and relaxation processes are shown schematically. Figure 6(a) depicts the PLE and PL spectra of 1.0 mol% Eu^{3+} doped $BiPO_4$ nanophosphor. From the excitation spectrum six excitation bands are identified which can be assigned to the electronic transitions of $^7F_0 \rightarrow {}^5D_4$ at 362 nm, $^7F_0 \rightarrow {}^5L_7$ at 381 nm, $^7F_0 \rightarrow {}^5L_6$ at 394 nm, $^7F_0 \rightarrow {}^5D_3$ at 415 nm, $^7F_0 \rightarrow {}^5D_2$ at 464 nm, and $^7F_0 \rightarrow {}^5D_1$ at 525 nm, including a charge transfer band (Eu–O charge transfer process) at 318 nm [39]. Only the prominent excitation peak at 394 nm has been selected for the measurement of room temperature emission spectrum of Eu^{3+} doped nanophosphor and clearly validates the fingerprint transition lines between the $^5D_0$ and $^7F_{J(J=0-4)}$ multiplets of the Eu^{3+} ion (Figure 6(a)). The

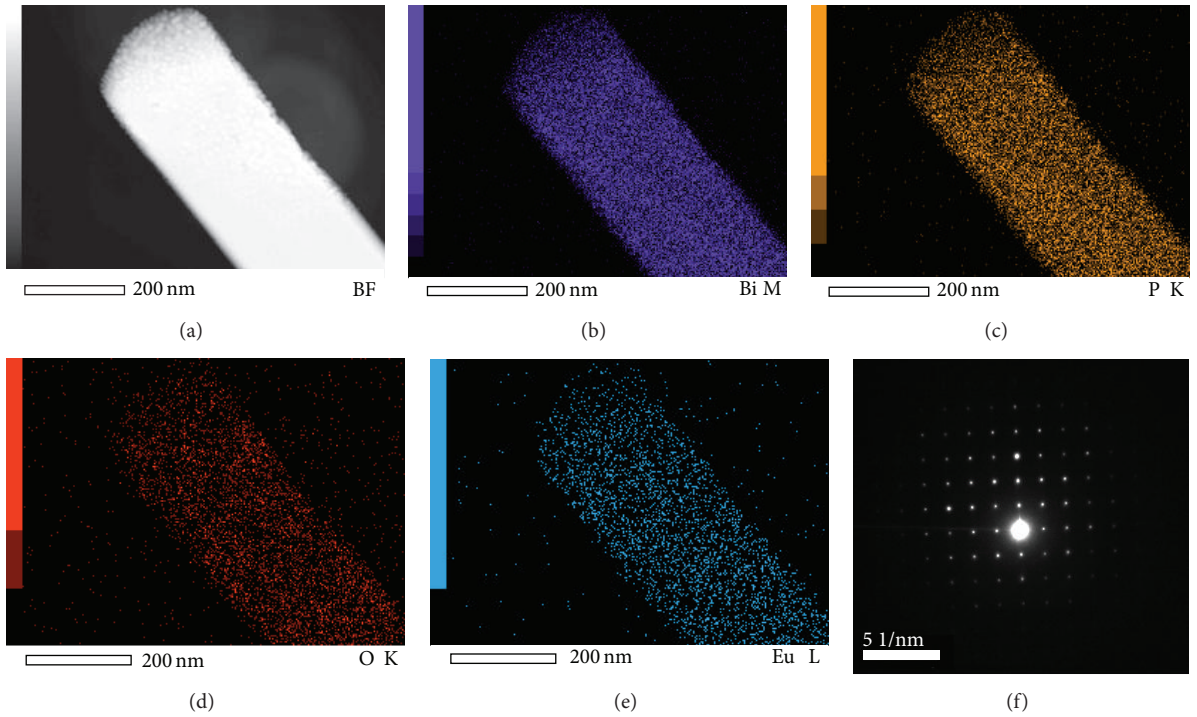

FIGURE 3: (a) Bright field TEM micrograph of the 1.0 mol% Eu^{3+} doped sample, (b) to (e) EDAX elemental mapping of Bi, P, O, and Eu. (f) Corresponding selected area electron diffraction pattern (SAED) with scale bar 5 nm.

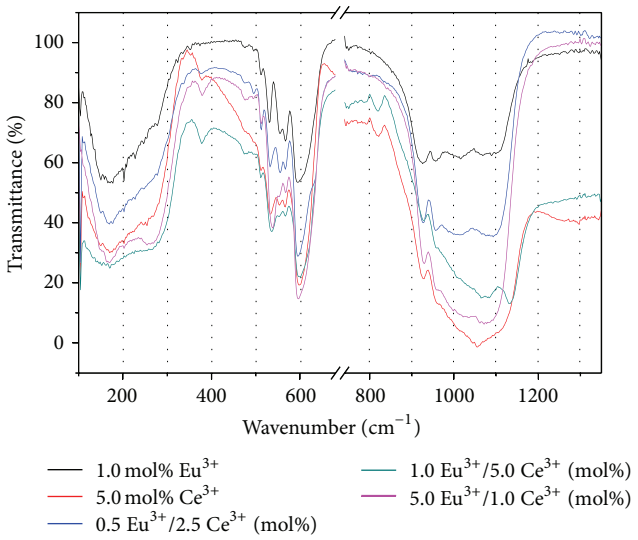

FIGURE 4: FTIR spectra of all the synthesized samples.

main emission line from the europium occurred in the yellowish-orange region at 595 nm, corresponding to the parity allowed magnetic dipole induced $^5D_0 \rightarrow {}^7F_1$ transition. Also, several other emission lines are observed from the Eu^{3+} luminescence spectrum which can be ascribed to the following transitions: 580 nm, the strictly forbidden $^5D_0 \rightarrow {}^7F_0$; 615 nm, and 622 nm, electric dipole allowed $^5D_0 \rightarrow {}^7F_2$ transition, 653 nm, a weak mixed character $^5D_0 \rightarrow {}^7F_3$; 688 nm, and 714 nm, the electric dipole allowed $^5D_0 \rightarrow {}^7F_4$ [21]. The intensity of an emission line is proportional to the radiative decay of the transition. It is well known that the probability of the $^5D_0 \rightarrow {}^7F_2$ transition is very sensitive to the changes in the chemical surroundings of the Eu^{3+} ions in the host matrix and its intensity is significantly affected by the degree in the center of symmetry in the environments around Eu^{3+} ions. The number of transitions between the nondegenerate $^5D_0$ and $^7F_0$ multiplets is usually used to estimate the number of Eu^{3+} sites in a crystalline lattice. In our study, the luminescence lines that are assigned to $^5D_0 \rightarrow {}^7F_2$ transition and $^5D_0 \rightarrow {}^7F_4$ transition of Eu^{3+} show the doublet-structure, and the lower symmetry sites induce the emission line splitting into doublet. When the Eu^{3+} ion is excited to $^5L_6$ level under 394 nm wavelength, it nonradiatively relaxes to the main emitting level $^5D_0$. From the $^5D_0$ level the Eu^{3+} ions decay radiatively, since the large energy difference of the $^7F_6$ level presents possibility of multiphonon relaxation as shown in the energy level scheme (Figure 6(b)). Based on the Dexters theory of resonant energy transfer [40], in solids two luminescence centers within a certain distance will be in resonance with each other and could transfer the excitation energy from one center (donor) to another center (acceptor). The close proximity of the centers enables them to be connected by electrostatic interaction or by the quantum mechanical exchange interaction. Also, for effective energy transfer, the emission of the donors must be overlapped with the absorption of the acceptors [41]. To examine possible energy transfer process between Ce^{3+} and Eu^{3+} or vice versa,

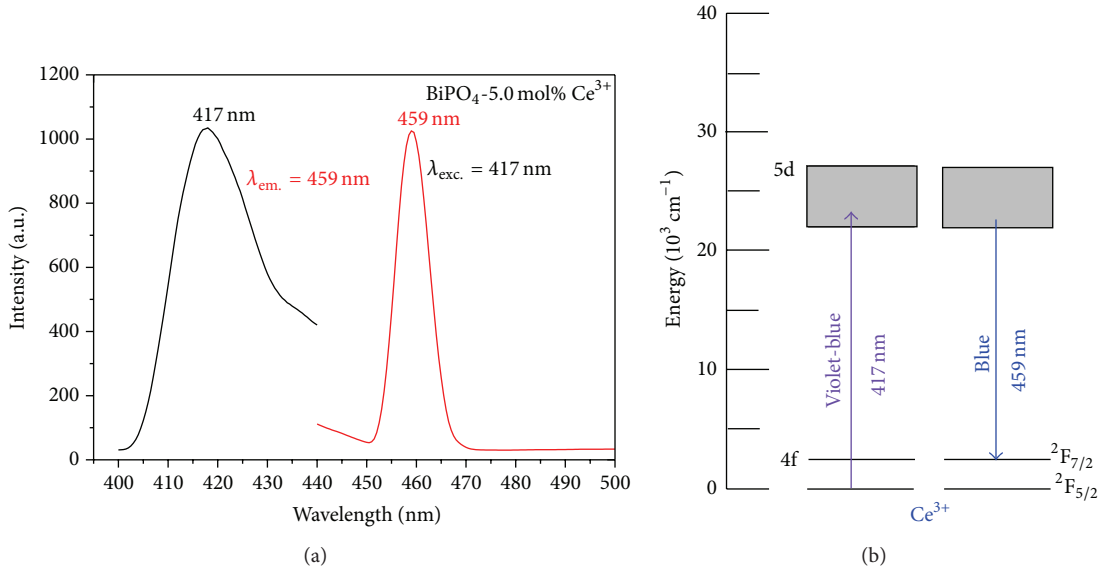

Figure 5: (a) PLE and PL spectra of 5.0 mol% singly Ce^{3+} doped sample and (b) corresponding energy level diagram.

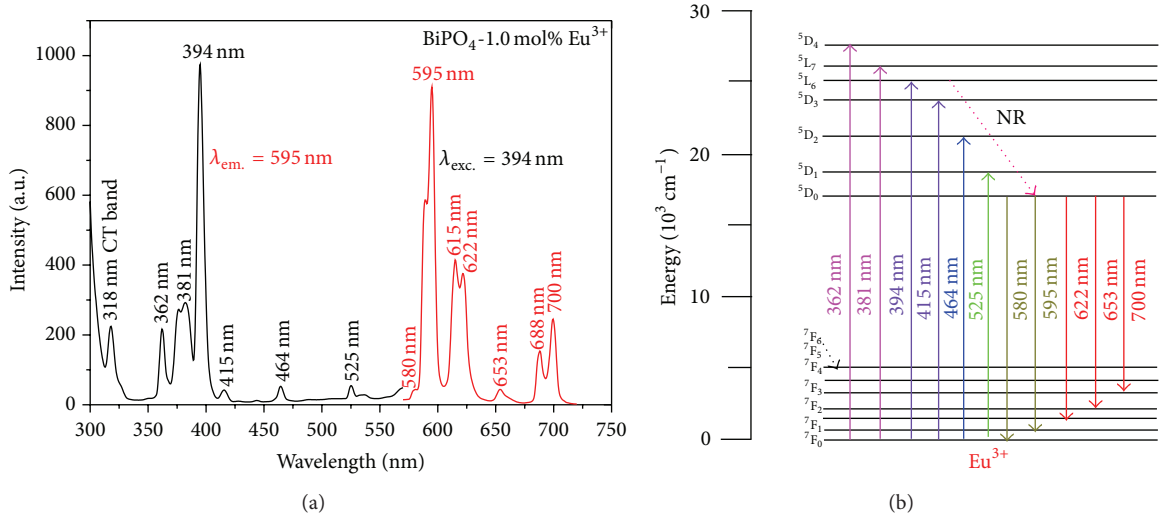

Figure 6: (a) PLE and PL spectra of 1.0 mol% singly Eu^{3+} doped sample and (b) corresponding energy level diagram.

in Figure 7(a) we present the comparison of Ce^{3+} emission and Eu^{3+} excitation spectra in $BiPO_4$ nanostructures. From this figure, one can hardly see any overlap between these spectra. This means that the emission of Ce^{3+} does not effectively overlap with the excitation spectrum of Eu^{3+} in synthesized $BiPO_4$ nanophosphors. Therefore, there is no possibility for energy transfer from Ce^{3+} to Eu^{3+} or vice versa in our synthesized $BiPO_4$: Ce/Eu codoped nanostructures (following Figures 5 and 6 one can see no spectral overlap between the emission and excitation band of the energy donor (Eu^{3+}) and the energy acceptor (Ce^{3+}), resp., for ET to occur from $Eu^{3+} \rightarrow Ce^{3+}$). Also, why Ce^{3+}/Eu^{3+} is not a good sensitizer/activator pair is clearly explained in [42] with some fundamental reasons apart from the possible lack of spectral overlap between them. Figures 7(b) and 7(c) present the PLE and PL spectra of Eu^{3+}/Ce^{3+} codoped nanophosphors with their respective excitation wavelengths 394 nm and 417 nm. At 394 nm only Eu^{3+} ions could be excited to higher levels, and Ce^{3+} ions stay inactive under this excitation wavelength. Similarly, at 417 nm only Ce^{3+} ions are excited. However, recently some other researchers [43] have reported energy transfer between Ce^{3+} and Eu^{3+} ions in silicate phosphors synthesized through a wet-chemistry method. From Figures 7(b) and 7(c), the characteristic emission bands of Eu^{3+} and Ce^{3+} ions are identified under their respective excitation wavelengths. By monitoring the emission at 459 nm (Ce^{3+}), the measured excitation spectrum did not show any excitation bands related to Eu^{3+} ion between 300 nm and 400 nm (Figure 7(c)). In the corresponding emission spectrum of Ce^{3+} between 500 nm and 750 nm no emission bands of

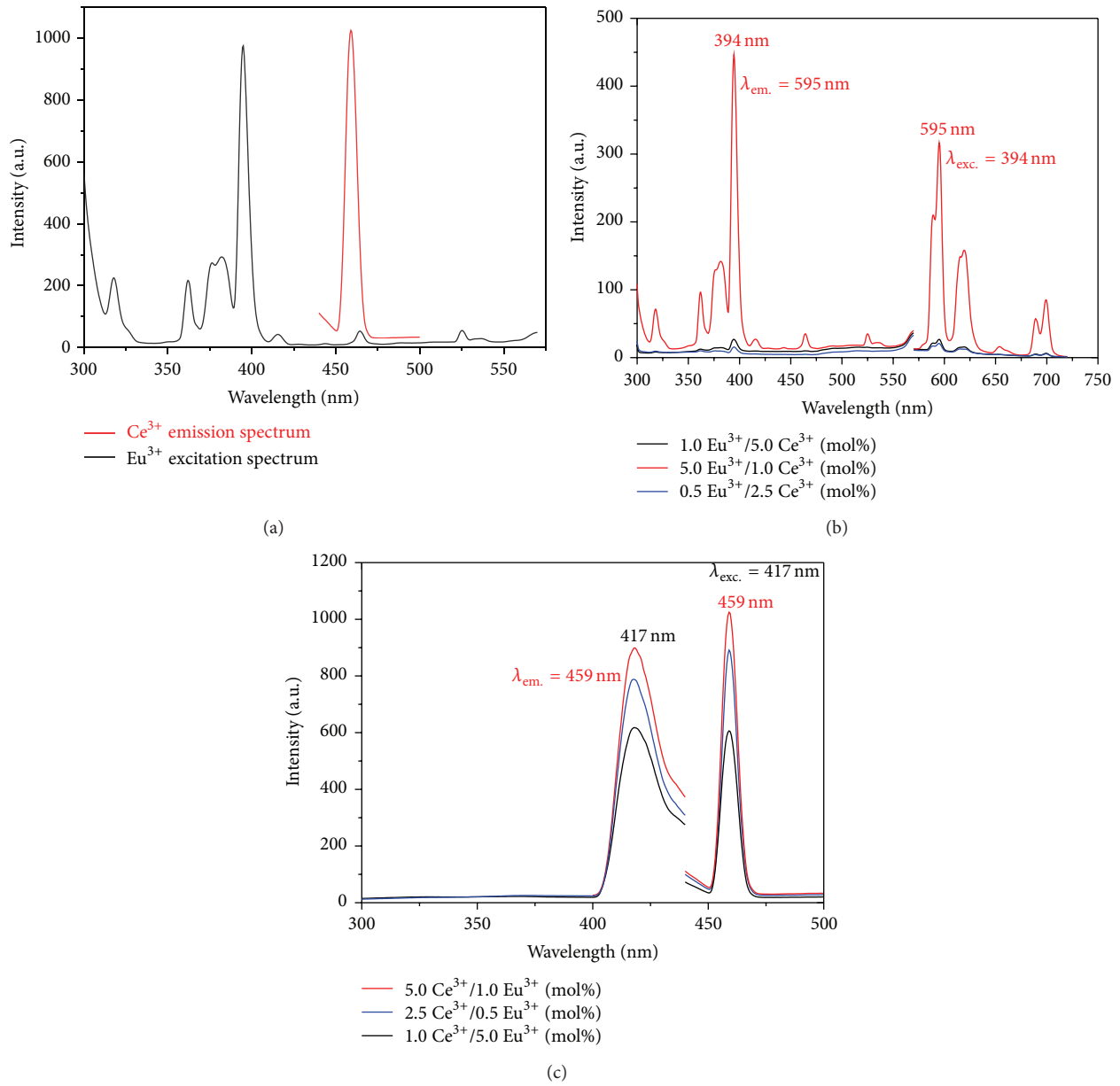

FIGURE 7: (a) Comparison of Eu^{3+}: excitation spectrum and Ce^{3+}: emission spectrum, (b) and (c) PLE and PL spectra of all the Ce^{3+}/Eu^{3+} codoped samples with 394 nm, and 417 nm excitation wavelengths.

Eu^{3+} are observed under 417 nm excitation wavelength except straight lines as shown in Figure 7(c) between 475 nm and 500 nm and this is obvious due to the absence of Eu^{3+} excitation bands under 459 nm monitored emission of Ce^{3+}. To show clearly the blue emission band of Ce^{3+} in Figure 7(c), we have provided the emission wavelength range up to 500 nm. However in all the Ce^{3+}/Eu^{3+} codoped samples we have observed independent dual emissions 459 nm (blue) and 594 nm (yellowish-orange) by externally varying excitation wavelengths as 417 nm and 394 nm. The relative emission intensity increases with doping concentration increment up to 5.0 mol% for both Eu^{3+} and Ce^{3+} and no concentration quenching occurred up to 5.0 mol% for either ions. For studying energy transfer between Ce^{3+} to Eu^{3+} ions, we have also measured the life times of Ce^{3+} single doped and Ce^{3+}/Eu^{3+} codoped samples using 370 nm excitation source (graph not shown). Life times of both samples were obtained by using double exponentials. Two life times with similar values for both singly and codoped samples were obtained at around 6.5 ± 0.6 ns and 186 ± 3 ns. Similar life time values for singly and codoped samples suggest minimum or no energy transfer in codoped samples. Earlier some researchers [22–28] have reported excitation dependent tunable emission in different systems like chitosan capped ZnS : Mn quantum dots, lanthanide doped metal organic frameworks, mixed lanthanide complexes, CdSe/ZnS quantum dots, nanocolloids

of ZnO, and graphene oxide. Some of them have reported this fluorescence behavior in violation of Kasha's rule of excitation wavelength independence [44]. They have given possible mechanism for this fluorescence behavior along with its application in multicolor bioimaging and lightning. Our results show that with careful adjustment of excitation wavelength, the color of luminescence can be modulated from blue to orange in same sample without changing its chemical composition and size. As discussed above nontransfer of energy among Ce^{3+}/Eu^{3+} dopants generates this excitation induced tunable emission. Here this tunable emission is achieved from nontoxic inorganic host material which is chemically and thermally stable. Thus synthesized codoped $BiPO_4$ nanostructures could be highly suitable for their practical applications in multicolor bioimaging, optoelectronics, and display devices.

4. Conclusions

In summary, bismuth phosphate ($BiPO_4$) nanophosphors doped with Ce^{3+} and Eu^{3+} ions singly and Ce^{3+}/Eu^{3+} codoped were prepared and their structural (XRD and FTIR), morphological (SEM-EDAX and TEM), and luminescence (PLE/PL) properties were studied. The synthesized lanthanides doped nanophosphors show pure hexagonal phase from XRD, SEM, and TEM analysis and expected phonon vibrational features attributed to the single-crystalline bismuth phosphate are found from the FTIR spectra. The incorporation of lanthanide ions into $BiPO_4$ crystalline hexagonal structure is also evident from the studied XRD profiles. The Ce^{3+} doped nanophosphors show 5d $\rightarrow$ $4f(^2F_{7/2})$ blue luminescence at 459 nm under excitation wavelength at 417 nm. For Eu^{3+} doped nanophosphors, five emission bands centered at 580 nm, 595 nm, (615 nm and 622 nm), 653 nm, and (688 nm, 700 nm) have been observed with 394 nm ($^5D_0 \rightarrow {}^7L_6$) excitation wavelength which can be assigned to ($^5D_0 \rightarrow {}^7F_{J(=0-4)}$) transitions. Among these emissions, $^5D_0 \rightarrow {}^7F_1$ transition shows bright yellowish-orange emission. No energy transfer was observed from either Ce^{3+} to Eu^{3+} or Eu^{3+} to Ce^{3+} in the Ce^{3+}/Eu^{3+} codoped $BiPO_4$ nanophosphors due to the absence of suitable common metastable excitation level for Ce^{3+} and Eu^{3+} ions at 417 nm or 394 nm to excite both ions simultaneously for a possible energy transfer (ET) between Ce^{3+} and Eu^{3+} ions. Also there is lack of considerable spectral overlap between Ce^{3+} emission spectrum and Eu^{3+} excitation spectrum for ET to take place and vice versa. Ce^{3+}/Eu^{3+} codoped $BiPO_4$ nanophosphors show excitation wavelength dependent tunable emission in blue (459 nm) and orange (594 nm) region by suitably varying excitation wavelength from 394 nm to 417 nm in single sample without varying chemical composition or size of nanomaterials.

Conflict of Interests

The authors declare that there is no conflict of interests regarding the publication of this paper.

References

[1] K. Iitaka, Y. Tani, and Y. Umezawa, "Orthophosphate ion-sensors based on a quartz-crystal microbalance coated with insoluble orthophosphate salts," *Analytica Chimica Acta*, vol. 338, no. 1-2, pp. 77–87, 1997.

[2] M. M. Charyulu, K. V. Chetty, D. G. Phal et al., "Recovery of americium from nitric acid solutions containing calcium by different co-precipitation methods," *Journal of Radioanalytical and Nuclear Chemistry*, vol. 251, no. 1, pp. 153–154, 2002.

[3] T.-S. Chang, L. Guijia, C.-H. Shin, Y. K. Lee, and S.-S. Yun, "Catalytic behavior of $BiPO_4$ in the multicomponent bismuth phosphate system on the propylene ammoxidation," *Catalysis Letters*, vol. 68, no. 3-4, pp. 229–234, 2000.

[4] G. Li, Y. Ding, Y. Zhang, Z. Lu, H. Sun, and R. Chen, "Microwave synthesis of $BiPO_4$ nanostructures and their morphology-dependent photocatalytic performances," *Journal of Colloid and Interface Science*, vol. 363, no. 2, pp. 497–503, 2011.

[5] M. Elmoudane, M. Et-Tabirou, and M. Hafid, "Glass-forming region in the system Li_3PO_4–$Pb_3(PO_4)_2$–$BiPO_4$ (Li_2O–PbO-Bi_2O_3–P_2O_5) and its ionic conductivity," *Materials Research Bulletin*, vol. 35, no. 2, pp. 279–287, 2000.

[6] L. Li, J. Xu, C. Guo, and Y. Zhang, "Removal of rhodamine B from aqueous solution by $BIPO_4$ hierarchical architecture," *Frontiers of Environmental Science and Engineering*, vol. 7, no. 3, pp. 382–387, 2013.

[7] Y.-F. Lin, H.-W. Chang, S.-Y. Lu, and C. W. Liu, "Preparation, characterization, and electrophysical properties of nanostructured $BiPO_4$ and Bi_2Se_3 derived from a structurally characterized, single-source precursor $Bi[Se_2P(OiPr)_2]_3$," *Journal of Physical Chemistry C*, vol. 111, no. 50, pp. 18538–18544, 2007.

[8] J. Geng, W.-H. Hou, Y.-N. Lv, J.-J. Zhu, and H.-Y. Chen, "One-dimensional $BiPO_4$ nanorods and two-dimensional BiOCl lamellae: fast low-temperature sonochemical synthesis, characterization, and growth mechanism," *Inorganic Chemistry*, vol. 44, no. 23, pp. 8503–8509, 2005.

[9] M. Guan, J. Sun, F. Tao, and Z. Xu, "A host crystal for the rare-earth ion dopants: synthesis of pure and ln-doped urchinlike $BiPO_4$ structure and its photoluminescence," *Crystal Growth and Design*, vol. 8, no. 8, pp. 2694–2697, 2008.

[10] M. Zhao, G. Li, J. Zheng, L. Li, H. Wang, and L. Yang, "Preparation and polymorph-sensitive luminescence properties of $BiPO_4$:Eu, Part I: room-temperature reaction followed by a heat treatment," *CrystEngComm*, vol. 13, no. 20, pp. 6251–6257, 2011.

[11] P. Arunkumar, C. Jayajothi, D. Jeyakumar, and N. Lakshminarasimhan, "Structure-property relations in hexagonal and monoclinic $BiPO_4$:Eu^{3+} nanoparticles synthesized by polyol-mediated method," *RSC Advances*, vol. 2, no. 4, pp. 1477–1485, 2012.

[12] M. Roming and C. Feldmann, "Synthesis and characterization of nanoscaled $BiPO_4$ and $BiPO_4$:Tb," *Journal of Materials Science*, vol. 44, no. 5, pp. 1412–1415, 2009.

[13] B. S. Naidu, B. Vishwanadh, V. Sudarsan, and R. K. Vatsa, "$BiPO_4$: a better host for doping lanthanide ions," *Dalton Transactions*, vol. 41, no. 11, pp. 3194–3203, 2012.

[14] X. Han, G. Zhang, X. Qi et al., "Synthesis and luminescence properties of $BiPO_4$:Ce,Tb nanorods," *Journal of Luminescence*, vol. 152, pp. 37–39, 2014.

[15] A. Kucuk and A. G. Clare, "Optical properties of cerium and europium doped fluoroaluminate glasses," *Optical Materials*, vol. 13, no. 3, pp. 279–287, 1999.

[16] G. Lakshminarayana, E. M. Weis, A. C. Lira, U. Caldiño, D. J. Williams, and M. P. Hehlen, "Cross Relaxation in rare-earth-doped oxyfluoride glasses," *Journal of Luminescence*, vol. 139, pp. 132–142, 2013.

[17] C. Shen, Q. Yan, Y. Xu et al., "Luminescence behaviors of Ce^{3+} ions in chalcohalide glasses," *Journal of the American Ceramic Society*, vol. 93, no. 3, pp. 614–617, 2010.

[18] C. G. Zuo, A. X. Lu, L. G. Zhu, and W. Y. Long, "Luminescence of Ce^{3+} or Tb^{3+}," in *Advanced Materials Research*, pp. 468–471, 2011.

[19] Y.-C. Wu, Y.-C. Chen, D.-Y. Wang, C.-S. Lee, C.-C. Sun, and T.-M. Chen, "α-(Y,Gd)FS:Ce^{3+}: a novel red-emitting fluorosulfide phosphor for solid-state lighting," *Journal of Materials Chemistry*, vol. 21, no. 39, pp. 15163–15166, 2011.

[20] L. H. C. Andrade, S. M. Lima, M. L. Baesso et al., "Tunable light emission and similarities with garnet structure of Ce-doped LSCAS glass for white-light devices," *Journal of Alloys and Compounds*, vol. 510, no. 1, pp. 54–59, 2011.

[21] M. R. N. Soares, C. Nico, M. Peres et al., "Structural and optical properties of europium doped zirconia single crystals fibers grown by laser floating zone," *Journal of Applied Physics*, vol. 109, no. 1, Article ID 013516, 2011.

[22] M. Sharma, T. Jain, S. Singh, and O. P. Pandey, "Tunable emission in surface passivated Mn-ZnS nanophosphors and its application for Glucose sensing," *AIP Advances*, vol. 2, Article ID 012183, 2012.

[23] M. Sharma, S. Singh, and O. P. Pandey, "Excitation induced tunable emission in biocompatible chitosan capped ZnS nanophosphors," *Journal of Applied Physics*, vol. 107, no. 10, Article ID 104319, 2010.

[24] A. R. Ramya, S. Varughese, and M. L. P. Reddy, "Tunable white-light emission from mixed lanthanide (Eu^{3+}, Gd^{3+}, Tb^{3+}) coordination polymers derived from 4-(dipyridin-2-yl)aminobenzoate," *Dalton Transactions*, vol. 43, no. 28, p. 10940, 2014.

[25] L. Irimpan, B. Krishnan, V. P. N. Nampoori, and P. Radhakrishnan, "Linear and nonlinear optical characteristics of ZnO-SiO_2 nanocomposites," *Applied Optics*, vol. 47, no. 24, pp. 4345–4351, 2008.

[26] J. Hoy, P. J. Morrison, L. K. Steinberg, W. E. Buhro, and R. A. Loomis, "Excitation energy dependence of the photoluminescence quantum yields of core and core/shell quantum dots," *Journal of Physical Chemistry Letters*, vol. 4, no. 12, pp. 2053–2060, 2013.

[27] A. Pramanik, Z. Fan, S. R. Chavva, S. S. Sinha, and P. C. Ray, "Highly efficient and excitation tunable two-photon luminescence platform for targeted multi-color MDRB imaging using graphene oxide," *Scientific Reports*, vol. 4, article 6090, 2014.

[28] F. Zhang, P. Yan, H. Li, X. Zou, G. Hou, and G. Li, "Towards full-color-tunable emission of two component Eu(III)-doped Gd(III) coordination frameworks by the variation of excitation light," *Dalton Transactions*, vol. 43, no. 33, pp. 12574–12581, 2014.

[29] C. Pan and Y. Zhu, "Size-controlled synthesis of $BiPO_4$ nanocrystals for enhanced photocatalytic performance," *Journal of Materials Chemistry*, vol. 21, no. 12, pp. 4235–4241, 2011.

[30] R. C. L. Mooney-Slater, "Polymorphic forms of bismuth phosphate," *Zeitschrift für Kristallographie*, vol. 117, no. 5-6, pp. 371–385, 1962.

[31] S. G. Motke, S. P. Yawale, and S. S. Yawale, "Infrared spectra of zinc doped lead borate glasses," *Bulletin of Materials Science*, vol. 25, no. 1, pp. 75–78, 2002.

[32] A. Gritco, M. Moldovan, R. Grecu, and V. Simon, "Thermal and infrared analyses of aluminosilicate glass systems for dental implants," *Journal of Optoelectronics and Advanced Materials*, vol. 7, no. 6, pp. 2845–2847, 2005.

[33] H. Assaoudi and A. Ennaciri, "Vibrational spectra and structure of rare earth orthophosphates, weinschenkite type," *Spectrochimica Acta, Part A: Molecular and Biomolecular Spectroscopy*, vol. 53, no. 6, pp. 895–902, 1997.

[34] H. Assaaoudi, A. Ennaciri, and A. Rulmont, "Vibrational spectra of hydrated rare earth orthophosphates," *Vibrational Spectroscopy*, vol. 25, no. 1, pp. 81–90, 2001.

[35] K. Nakamoto, *Infrared and Raman Spectra of Inorganic and Coordination Compounds, Part A: Theory and Applications in Inorganic Chemistry*, John Wiley and Sons, New York, NY, USA, 5th edition, 1997.

[36] B. Romero, S. Bruque, M. A. G. Aranda, and J. E. Iglesias, "Syntheses, crystal structures, and characterization of bismuth phosphates," *Inorganic Chemistry*, vol. 33, no. 9, pp. 1869–1874, 1994.

[37] C.-H. Lu, H.-C. Hong, and R. Jagannathan, "Sol-gel synthesis and photoluminescent properties of cerium-ion doped yttrium aluminium garnet powders," *Journal of Materials Chemistry*, vol. 12, no. 8, pp. 2525–2530, 2002.

[38] G. Blasse and A. Bril, "Investigation of some Ce^{3+}-activated phosphors," *The Journal of Chemical Physics*, vol. 47, no. 12, pp. 5139–5145, 1967.

[39] G. Lakshminarayana and S. Buddhudu, "Spectral analysis of Eu^{3+} and Tb^{3+}:B_2O_3-ZnO-PbO glasses," *Materials Chemistry and Physics*, vol. 102, no. 2-3, pp. 181–186, 2007.

[40] D. L. Dexter, "A theory of sensitized luminescence in solids," *The Journal of Chemical Physics*, vol. 21, no. 5, pp. 836–850, 1953.

[41] G. Lakshminarayana and L. Wondraczek, "Photoluminescence and energy transfer in Tb^{3+}/Mn^{2+} co-doped $ZnAl_2O_4$ glass ceramics," *Journal of Solid State Chemistry*, vol. 184, no. 8, pp. 1931–1938, 2011.

[42] W. M. Yen, H. Yamamoto, and S. Shionoya, *Phosphor Handbook*, CRC Press, Taylor & Francis, Oxford, UK, 2nd edition, 2006.

[43] O. M. Ntwaeaborwa, H. C. Swart, R. E. Kroon, P. H. Holloway, and J. R. Botha, "Photoluminescence and energy transfer in Tb^{3+}/Mn^{2+} co-doped $ZnAl_2O_4$ glass ceramics," *Surface and Interface Analysis*, vol. 38, pp. 458–461, 2006.

[44] J. B. Birks, *Photophysics of Aromatic Molecules*, John Wiley & Sons, New York, NY, USA, 1970.